# Image Appraisal of Full Waveform Inverted GPR Data

**G. Meles[1], S. Greenhalgh[2], H. Maurer[2], and A. Green[2]**

[1]School of Geosciences, University of Edinburgh
The Kings Buildings, West Mains Road, Edinburgh EH9 3JN, UK
[2]Institute of Geophysics, ETH Zurich, Sonneggstrasse 5, CH 8092 Zurich, Switzerland

**Abstract**— We have recently developed a novel method for explicitly computing the permittivity $\varepsilon$ and conductivity $\sigma$ sensitivity functions (Jacobian matrix $\mathbf{J}$) of ground penetrating radar (GPR) data, based on a time domain adjoint approach which uses a finite difference modeling method. This not only opens up the possibility for performing Gauss-Newton type inversions, which offer distinct advantages over standard gradient-based approaches, but also permits a methodology for assessing the reliability of inverted GPR images from full waveform data. Image appraisal is performed through a joint analysis of the eigenvalue spectrum of the pseudo Hessian matrix $\mathbf{H} = \mathbf{J}^T\mathbf{J}$ and the formal model resolution matrix $\mathbf{R} = (\mathbf{J}^T\mathbf{J} + \lambda\mathbf{I})^{-1}\mathbf{J}^T\mathbf{J}$, where $\lambda$ is a damping value to stabilize the matrix inversion. In seismic and geoelectric inversion, the damping factor is often chosen as the median value of $\mathbf{H}$, but the justification for this is not clear. The diagonal values of $\mathbf{R}$ give the resolution of each cell in the model, with values varying from 0 (unresolved) to 1 (perfectly resolved). The off-diagonal elements convey the trade-offs (cross-coupling) between the different parameters, and the degree of image blurring. The eigenvalue distribution of the pseudo-Hessian matrix provides a measure of the information content of an experiment and shows the unresolved model space. The effect of model perturbation along a given eigenvector direction on the cost function is established in terms of the size of the corresponding eigenvalue. The relative eigenvalue range (RER), which is the width of the normalized spectrum (with entries assembled in descending eigenvalue order) at the level of the noise floor, is a measure of the resolved model space. Four and three-sided radar acquisition geometries (e.g., combination crosshole and borehole-to-surface) yield higher RER values than a one-sided (surface reflection) or two-sided (crosshole) experiment, indicating greater information content and smaller null spaces. Clearly, the better the angular and spatial coverage of the target, the more reliable the image. Resolution is not just a function of the recording geometry and the quantity measured but also the underlying model itself.

We show that cumulative sensitivity (i.e., the column sum of absolute values of the Jacobian) images can be used as a reasonable proxy for formal resolution. Cumulative sensitivity is far less expensive than obtaining the resolution matrix, which involves large matrix inversion and multiplication. We also show that only minor differences exist between the resolution images provided by normalized Jacobians for the full set of $\varepsilon$ and $\sigma$ parameters and the sub-Jacobians for the individual $\varepsilon$ and $\sigma$ values. Permittivity sensitivity values are typically $10^9$ times larger than the conductivity values, because they involve a time derivative of the electric field ($i2\pi f$ term, where frequency $f$ is $\sim 100\,\mathrm{MHz}$) as opposed the field itself. Without normalization of sensitivities or using sub-Jacobians, conductivity updating would be impossible.

To provide more insightful meaning to resolution, we have undertaken a singular value decomposition of the pseudo-Hessian matrix $\mathbf{W}\Omega\mathbf{D}^T = \mathbf{H}$ and then extract the eigenvectors of $\mathbf{D}$ corresponding to the 'a' largest singular values (because $H$ is self adjoint, these are identical to the eigenvalues) of $\Omega$: $\mathbf{A}_{ij} = \mathbf{D}_{ij}$, $i = (1, 2, \ldots, M)$; $j = (1, 2, \ldots, a < M)$. We then form an alternative expression for the resolution matrix $\mathbf{R}^a = \mathbf{A}\mathbf{A}^T$ and take the diagonal elements of $R^a$ as representative of resolution in each cell. There is a close relationship between resolution provided by $\mathbf{R}$ and $\mathbf{R}^a$. The effect of the damping factor $\lambda$ in the formal model resolution formula for $\mathbf{R}$ is basically equivalent to the role of $a$ in the truncated SVD resolution $\mathbf{R}^a$. Small values of $\lambda$ have a very similar effect as choosing small values of $a$. (i.e., just the most dominant eigenvalues). Since SVD resolution is clearly connected to the spectrum of the Hessian, and because the singular values of $\Omega$ and the eigenvalues of $\mathbf{H}$ are identical, it provides insight and guidance on the effect of damping in computing $\mathbf{R}$. However, SVD analysis is extremely expensive from a computational point of view and not intended for routine applications.

In this contribution we illustrate the sensitivity patterns, eigenvalue spectra and resolution plots for a variety of heterogeneous models and recording setups.

## 1. INTRODUCTION

Most waveform inversions of ground penetrating radar (GPR) data [1] are based on gradient methods [5] that are less expensive computationally than Gauss-Newton or full Newton approaches [3, 4],

because they do not require the inversion of large matrices in the updating process. A critical aspect of any inversion procedure is the assessment of the reliability of the final image. Most often, mere convergence in the data space (i.e., the matching of observed and synthetic GPR traces) is the only criterion used to appraise the goodness of a final result. A better indication of the correctness of an inverted model could be obtained by means of a formal model resolution analysis [3]. This requires the computation of the sensitivity or Jacobian matrix. We recently developed an efficientand novel scheme for computing the permittivity and conductivity sensitivity functions explicitly based on a time-domain adjointmethod [2]. The Fréchet derivatives, which form elements of the Jacobian matrix, are obtained by cross correlating forward propagated fields and backward propagated Green's functions from the receiver positions (adjoint sources). The procedure was implemented usinga standard finite difference time domain modeling method.

The availability of the Jacobian not only enables formal resolution analysis to be undertaken but also Gauss-Newton style inversions to be performed, which generally converge faster than gradient approaches. In addition, it opens up the possibility to carry out an information content analysis of the radar data by singular value decomposition of the Jacobian (or what is equivalent, an eigenvalue analysis of the pseudo (approximate) Hessian matrix). The eigenvalue spectrum is a useful tool in experimental design because it conveys the extent of the resolved model space and permits comparison of the efficacy of different recording configurations and data sets.

## 2. EXPLICIT EXPRESSIONS FOR THE SENSITIVITY KERNELS

The GPR sensitivity functions for each model cell or block in the subsurface are a measure of how a perturbation in the electrical property (permittivity $\varepsilon$ or conductivity $\sigma$) in that cell causes a perturbation in the measured electric field for a given radar transmitter-receiver configuration. The explicit formulae for the columns of the sensitivity functions for any receiver location $\mathbf{x}_r$ and observation time $t_r$ were derived in [2] and can be stated thus:

$$\left[\mathbf{J}_\varepsilon^S(x')\right]_{x_r,t_r}^i = \left\langle \delta\left(\mathbf{x} - \mathbf{x}'\right) \partial_t \mathbf{E}^S, \mathbf{G}^T \delta^i\left(\mathbf{x} - \mathbf{x}_r, t - t_r\right)\right\rangle \tag{1}$$

$$\left[\mathbf{J}_\sigma^S(x')\right]_{x_r,t_r}^i = \left\langle \delta\left(\mathbf{x} - \mathbf{x}'\right) \mathbf{E}^S, \mathbf{G}^T \delta^i\left(\mathbf{x} - \mathbf{x}_r, t - t_r\right)\right\rangle \tag{2}$$

where the bracket symbol $\langle\rangle$ indicates inner product. Here the superscript $i$ indicates the individual vectorial components , the subscripts $\varepsilon$ and $\sigma$ denote either a permittivity or conductivity derivative, $\mathbf{x}'$ is any domain point, $\mathbf{E}^S$ is the electric field in the whole space-time domain, $\mathbf{G}$ is the Green's operator, $T$ indicates transposition, and the superscript 's' on $E$ refers to a particular source. We now concentrate on the right side term $\mathbf{G}^T\delta^i(\mathbf{x} - \mathbf{x}_r, t - t_r)$ in Eqs. (1)and (2) where the adjoint source at the receiver has a single component (i.e., electric dipole direction) that corresponds to the same component of the sensitivity in which we are interested, namely $\partial E^i(x_r, t_r)/\partial\varepsilon(x')$ or $\partial E^i(x_r, t_r)/\partial\sigma(x')$. The inner products in (1) and (2) involve an integration over space and time. In these equations, the argument of the delta function, $\mathbf{x} - \mathbf{x}'$, indicates the point at which we are computing the sensitivities. The dummy variables over which the integration implicit in (1) and (2) takes place are indicated in the following by $x^*$ and $t^*$.

$$\left[G^T\delta(x - x_r, t - t_r)_{x*,t*}^i\right]^j = G^{ij}(x^*, t_r, x_r, t^*) \tag{3}$$

The inner product sums over the $j$ different field components, which are forward and back propagated in (1) and (2). Due to reciprocity (3) can be written as

$$\left[\mathbf{G}^T\delta(x - x_r, t - t_r)_{x*,t*}^i\right]^j = G^{ji}(x^*, t_r, x_r, t^*) \tag{4}$$

These are the different components of the wavefield generated by the delta-function source oriented along a single direction $i$. From time invariance, we can write (3) as:

$$G^{ji}(x^*, t_r, x_r, t^*) = G^{ji}(x^*, t_r - t^*, 0) \tag{5}$$

The computation of (5) involves the solution of a standard forward problem, with the source placed at $x_r$ and discharged at $t = 0$. Depending on the value of $t_r$, different wavefields $G^{ji}(x^*, t_r - t^*, x_r, 0)$ will be cross correlated with $\partial_t \mathbf{E}^s(x^*, t^*)$ and $\mathbf{E}^s(x^*, t^*)$. The presence of $\delta(\mathbf{x} - \mathbf{x}')$ in (1) and (2) reduces in practice the integration to that over time alone.

Practical issues of back propagating a Green's delta function in an FDTD scheme can be circumvented due to the orthogonality of the Fourier base (any frequency component not common to both vectors in an inner product has no effect on the result) so it is only necessary to back propagate a filtered delta function in accordance with the frequencies contained in the source spectrum [2].

The size of the Jacobian is $N \times M$, where $N$ is the total number of measurements (number of sources × number of receivers × number of times along each trace) and $M$ is the number of model parameters (number of cells ×2, if both permittivity and conductivity are considered). The temporal derivative of the electric field appearing in (1), suggests that the GPR permittivity sensitivities will be much higher (by $2\pi f$, $f \approx 100\,\mathrm{MHz}$) than the corresponding conductivity sensitivities (which depend on the electric field itself), and so it is necessary to normalize the Jacobian or work with sub-Jacobians for each class of model parameter.

Figures 1(a), (b) show a heterogeneous model involving two cross-shaped anomalous bodies embedded in a homogeneous background of relative permittivity $\varepsilon_r = 4$ and conductivity $\sigma = 3\,\mathrm{mS/m}$. Cross 1 is resistive ($\sigma = 0.1\,\mathrm{mS/m}$) with low $\varepsilon_r = 1$, whereas cross 2 is conductive ($\sigma = 10\,\mathrm{mS/m}$) with high $\varepsilon_r$. The waveform in Fig. 1(c) represents the GPR trace for the crossholecopolarized recording configuration as shown, with transmitter and receiver both located at a depth of 5.3 m and 10 m apart. Apart from the direct transmitted arrival, there are additional forward scattered signals present. Point A corresponds to the first arrival, B to an arbitrary relative
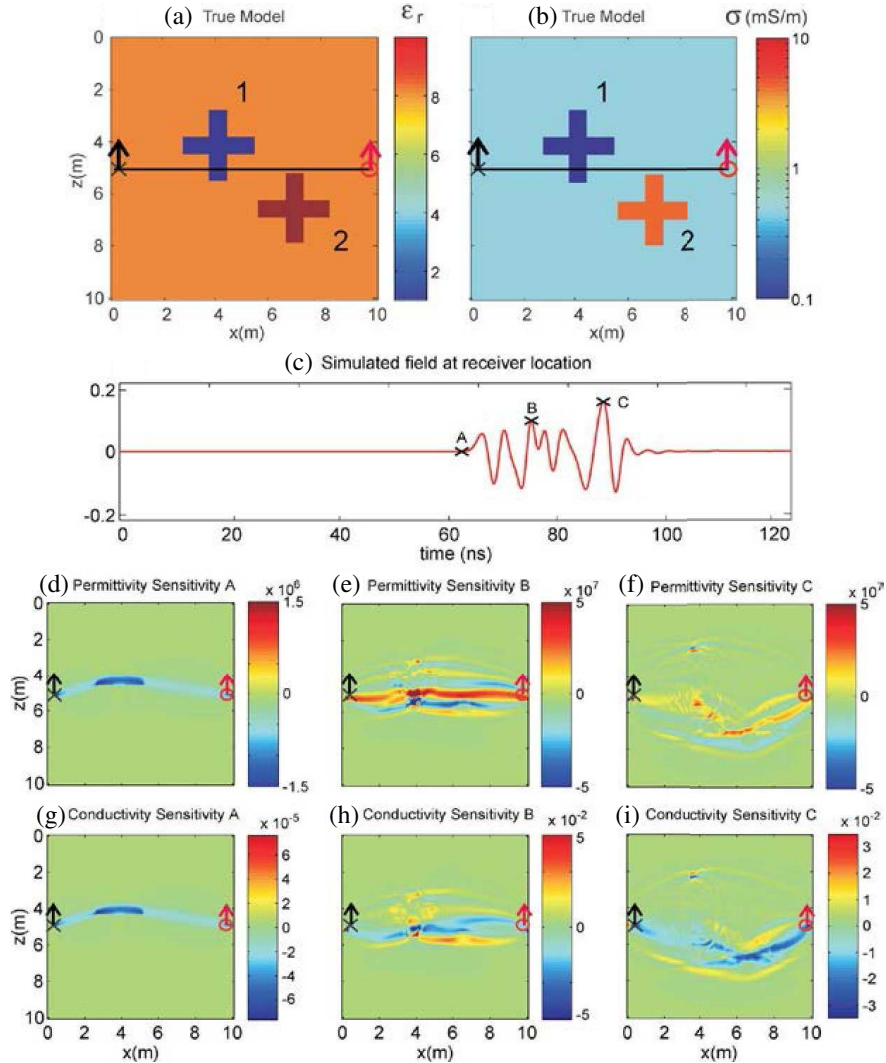


Figure 1: (a) Permittivity $\varepsilon$ and (b) conductivity $\sigma$ distributions for heterogeneous model. (c) Radar trace for Tx and Rx antennae positions as shown. (d)–(i) show the $\varepsilon$ and $\sigma$ sensitivity patterns for the three observation times A, B and C indicated in (c). Units of $\varepsilon$ permittivity sensitivity are $\mathrm{V^2/A \cdot s}$ and $\sigma$ sensitivity are $\mathrm{V^2/A}$.

amplitude maximum and C to the absolute maximum amplitude of the entire trace. The $\varepsilon$ and $\sigma$ sensitivities throughout the medium are shown in Figs. 1(d)–(f) and 1(g)–(i) for these three time samples A, B and C. There are significant amplitude differences between the pairs of corresponding sensitivity plots. The sensitivity patterns are significantly distorted from the quasi-elliptical shape expected in a homogenous medium. As time increases, the sensitivity patterns expand to occupy a larger region of the model.

## 3. INFORMATION CONTENT ANALYSIS

The availability of the Jacobian values for various receiver locations and observation times (Eqs. (1) and (2)) also allows the computation of the pseudo-Hessian matrix, given by $\mathbf{H}^A = \mathbf{J}^T\mathbf{J}$. The size of this matrix is $M \times M$. The inverse of this matrix is used in Gauss-Newton inversion as a more refined version of a step length operator common in gradient based inversion schemes. It specifies the extent of model updating in the gradient direction. The eigenvalue spectrum of the pseudo Hessian also reveals the information content of a data set, and can be used to appraise the imaging capability of different recording configurations. Fig. 2 shows in semi-log form the normalized eigenvalues, arranged in descending order, for the model of Fig. 1 but for four different recording configurations: surface, cross-hole, three-sided and four sided. The surface and crosshole experiments involve 5 transmitters and 5 receivers placed uniformly along the upper side of the model (surface case) or in the left and right sides of the model (crosshole), whereas for the 3-sided experiment 15 transmitters and 15 receivers are placed evenly along the upper and lateral sides of the model. For the 4-sided experiment, and additional 5 transmitters and 5 receivers are palced along the bottom side of the model. The three separate plots in Fig. 2 are for the complete model space ($\varepsilon$ and $\sigma$ together), and the separate model spaces ($\varepsilon$ only, and $\sigma$ only). The intersection of the eigenvalue spectra with the horizontal threshold line (relative eigenvalue $= 10^{-7}$) delineate the resolved model space and the mostly unresolved model space. This threshold corresponds to a noise floor below which no significance should be attached to the eignevalues. The portion to the left of the intersection point is referred to as the relative eigenvalue range (RER) and it provides a simple measure of the goodness of a particular experimental design. The increasing size of the RER for the four different experiments (with the highest for the 4 sided experiment) and second highest for the 3-sided experiment give a clear indication of the increasing reliability of the inverted models for the different configurations. This can be linked to the improved angular and spatial coverage of the target.
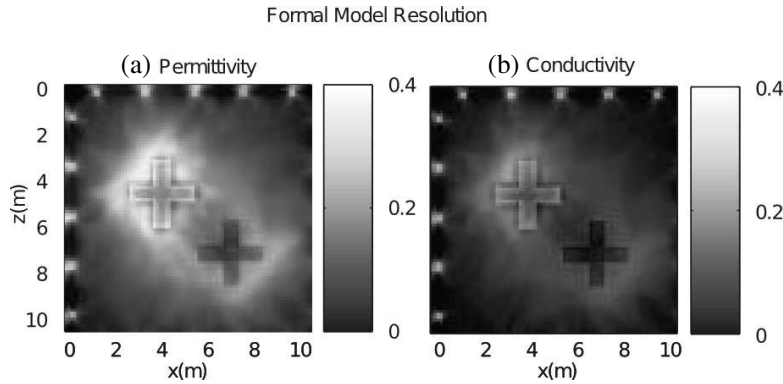


Figure 2: Formal model resolution for (a) permittivity and (b) conductivity for the four-sided experiment.

## 4. FORMAL RESOLUTION AND CUMULATIVE SENSITIVITY

The resolution of each cell within an inverted model can be expressed formally by the model resolution matrix $R$ defined as [3]:

$$\mathbf{R} = \left(\mathbf{J}^T\mathbf{J} + \lambda\mathbf{I}\right)^{-1}\mathbf{J}^T\mathbf{J} \tag{6}$$

where $\lambda$ is a damping factor (to ensure that the matrix can be inverted) and $\mathbf{I}$ is the identity matrix. $\mathbf{R}$ relates the estimated model parameters $m^{est}$ with the true model parameters $m^{true}$ through the relationship $m^{est} = Rm^{true}$. Of particular interest are the diagonal elements of $\mathbf{R}$. Values close

to 0 indicate poorly resolved parameters, whereas values close to 1 indicate well resolved model parameters. The rows of $\mathbf{R}$ indicate the degree of smearing or point spread functions for each cell.

Figure 3 shows the formal model resolution images obtained for the 4-sided experiment on the double cross model (Fig. 1) and described above. The two plots correspond to the permittivity and conductivity sub-Jacobians, and illustrate better resolution for the resistive and low permittivity cross.

A surrogate or proxy for assessing formal resolution is the cumulative sensitivity function, obtained by summing over all transmitters, receivers and observation times the absolute values of the sensitivities, i.e., a column sum of the Jacobian, given by:

$$\mathbf{CS}(m) = \sum_s \sum_r \sum_\tau |\mathbf{J}^s(m)||_{x_r, t_r} \tag{7}$$

The quantity CS is rarely used in GPR or seismic waveform inversion but its appeal is that it does not require any matrix multiplication or inversion, and is therefore relatively inexpensive. Space limitations preclude showing comparison CS plots to Fig. 3. Although differences exist there is a strong similarity in shape, and high cumulative sensitivity values are concentrated in the same regions of the model where formal resolution is high.
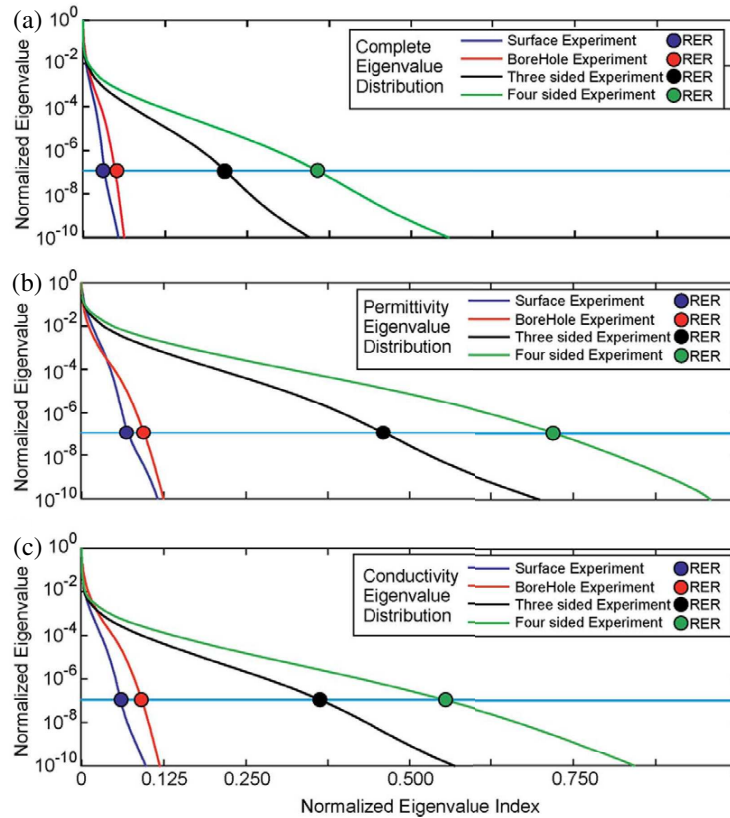


Figure 3: Eigenvalue spectra (a) $\varepsilon$ and $\sigma$ together, (b) $\varepsilon$ separate, and (c) $\sigma$ separate for the four different recording configurations.

## 5. SVD RESOLUTION

An alternative to the definition of formal resolution can be provided by means of a singular value decomposition (SVD) of the pseudo-Hessian matrix, given by

$$\mathbf{W}\mathbf{\Omega}\mathbf{D}^{\mathbf{T}} = \mathbf{H}^{\mathbf{A}} \tag{8}$$

and then extract the eigenvectors of $\mathbf{D}$ corresponding to the 'a' largest singular values (or eigenvalues) of $\Omega$:

$$A_{ij} = D_{ij}, \quad i = (1, 2, \ldots, M), \quad j = (1, 2, \ldots, a \ < \ M) \tag{9}$$

We then form the following alternative expression for the resolution matrix, referred to as SVD resolution:

$$\mathbf{R^a = AA^T} \tag{10}$$

and take the diagonal elements of $\mathbf{R^a}$ as representative of resolution in each cell. Values close to zero indicate poorly resolved model parameters, whereas values close to one indicate well-resolved model parameters. Both the natural model space and that expressed by the columns of $\mathbf{D}$ are orthonormal.

Each vector of the natural base, $m_i$, can be expressed as a linear combination of vectors in the orthonormal base provided by $\mathbf{D}$:

$$m_i = \sum_{k=1}^{M} c_k \mathbf{v}_k \tag{11}$$

where $\mathbf{v}_k$ are the othonormal columns of $\mathbf{D}$ and $c_k$ are the numerical coefficients of the $i$-th column of $\mathbf{D}^{-1}$. Since $\mathbf{D}^{-1} = \mathbf{D}^T$, it is straightforward to see that

$$R_{i,i}^a = \sum_{k=1}^{a} c_k^2 = \sum_{k=1}^{a} D_{ik}^2 \tag{12}$$

Because $\mathbf{D}$ consists of orthonormal columns, $R_{i,i}^a$ is always smaller than 1.

More specifically, the resolution valued defined in XX is equivalent to the relative amplitude of the projection of the natural base element $m_i$ on the space spanned by the eigenvectors corresponding to the $a$ largest singular values (i.e., the best resolved ones). There is a very close relationship between the resolution provided by (6) and (10). The effect of the damping factor in (6) is basically equivalent to the role of $a$. Small values of $\lambda$ correspond to large values of $a$, whereas large values of $\lambda$ have a very similar effect as choosing small values of $a$ (i.e., just the most dominant eigenvalues).

Since SVD resolution is clearly connected to the spectrum of the Hessian, and because the singular values of $\Omega$ and the eigenvalues of $\mathbf{H}^A$ are identical, it provides an insightful meaning to resolution. However, since SVD is extremely expensive from a computational point of view, and not intended for routine practical applications, formal resolution analysis is most often presented.

Figure 4 gives a comparison between formal resolution (6) and SVD resolution (10) for the same heterogeneous model comprising the two anomalous crosses. The upper set of diagrams (a)–(e) depict formal model resolution images for different choices of the damping factor $\lambda$, in the range 0.01 to 100 times the median value of the diagonal value of $\mathbf{H}^A$. By comparison, the bottom set of diagrams (f)–(j) show SVD resolution for different sets of eigenvalues ranging from the 80 largest ones to the 3000 largest ones (from a total of 7744). The (a)–(e) and (f)–(j) diagrams of Fig. 4 are extremely similar, establishing a tight connection between the two definitions of resolution.
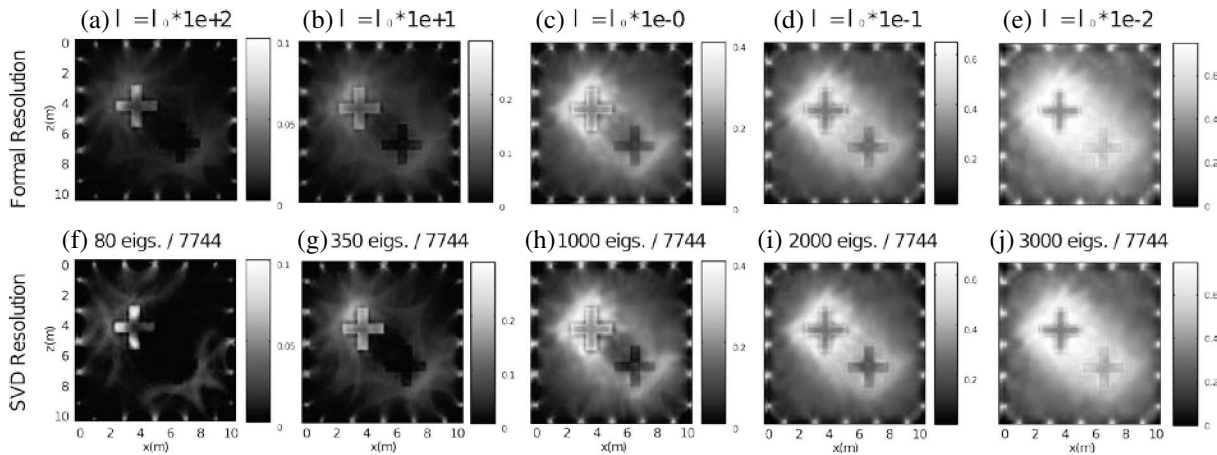


Figure 4: (a)–(e) Formal model resolution images for the 4-sided experiment and 5 different choices of the damping parameter $\lambda$. $\lambda_0$ corresponds to the median value of the diagonal elements of the pseudo-Hessian. (f)–(j) Corresponding SVD resolution for 5 different choices of the number of eigenvalues used for the definition of matrix $A$.

Moreover, the differences arising in these images as a function of the damping factor or the number of eigenvalues used suggests that particular care must be taken when analyzing resolution plots.

## 6. CONCLUSIONS

We have developed a new and effective method for calculating GPR sensitivity functions in the time domain. This allows us to assess the reliability of inverted images from GPR full waveform data and the adequacy of an experimental setup. The usual criterion of simple convergence in the data space is insufficient to appreciate the goodness of a model. Through an analysis based on the eigenvalue distribution of the Hessian, the cumulative sensitivity pattern and the formal or SVD resolution matrix it is possible to provide a meaningful estimate of the well resolved and poorly resolved features of an inverted image.

**REFERENCES**

1. Meles, G., S. A. Greenhalgh, J. van der Kruk, and A. G. Green, "Taming the non-linearity problem in GPR full-waveform inversion for high contrast media," *J. App. Geophys.*, Vol. 73, 174–186, 2011.
2. Meles, G., S. A. Greenhalgh, A. G. Green, H. Maurer, and J. van der Kruk, "GPR full waveform sensitivity and resolution analysis using an FDTD adjoint method," *IEEE Trans. Geosci. Remote Sensing*, Vol. 50, No. 5, 1881–1896, 2012.
3. Menke, W., *Geophysical Data Analysis. Discrete Inverse Theory*, Academic Press, London, 1989.
4. Pratt, R. G., C. Shin, and G. J. Hicks, "Gauss-Newton and full Newton methods in frequency-space seismic waveform inversion," *Geophys. J. Int.*, Vol. 133, No. 2, 341–362, 1998.
5. Tarantola, A., "Inverse problem theory and methods for model parameter estimation," SIAM: Society for Industrial and Applied Mathematics, 2004.